www.sciencemag.org/cgi/content/full/341/6141/53/DC1

Supplementary Materials for

A Population of Fast Radio Bursts at Cosmological Distances

D. Thornton,* B. Stappers, M. Bailes, B. Barsdell, S. Bates, N. D. R. Bhat, M. Burgay, S. Burke-Spolaor, D. Champion, P. Coster, N. D'Amico, A. Jameson, S. Johnston, M. Keith, M. Kramer, L. Levin, S. Milia, C. Ng, A. Possenti, W. van Straten

*Corresponding author. E-mail: thornton@jb.man.ac.uk

Published 5 July 2013, *Science* **341**, 53 (2013)
DOI: 10.1126/science.1236789

This PDF file includes:

Materials and Methods

The High Time Resolution Universe (HTRU) survey at Parkes is separated into high-, mid- and low-Galactic latitudes (*1*). These Fast Radio Bursts (FRBs) have been discovered in the high-latitude region that was designed to provide a snapshot of the transient radio sky (see Table S1).

The survey uses the 13-beam receiver at the prime focus of the 64-m Parkes radio telescope, New South Wales, Australia. Each beam has a half-power beam-width (HPBW) at 1.3 GHz of approximately 14 arcminutes. Adjacent beam centers are separated by approximately 2 HPBW and as such a single pointing of the telescope does not cover a patch of sky at the HPBW gain level. Consequently, when an FRB is detected in a single beam the closest simultaneously observed beam centers are 2 HPBWs away. Multiple telescope pointings are required to fully sample the sky (*1*).

The mid-latitude part of the survey has been completed, while observations for the low- and high-latitude regions are ongoing at the time of writing. The search for single pulses in the high-latitude region has covered 95,670 individual beams each observed for 270 seconds. This corresponds to 24% of the survey region and almost 11% of the full sky; it is in this data set that the FRBs were found. The processed high-latitude beams are concentrated in the region $-70° < b < -30°$ corresponding to lines of sight with low Milky Way (MW) contributions to dispersion measure (DM) and scattering.

The digital back-end 8-bit samples two polarizations from each beam, the sum of these two values is then 2-bit sampled. This is done across 1024 frequency channels every 64 μs. The data are recorded to tape and sent to Jodrell Bank Centre for Astrophysics and Swinburne University of Technology for processing and searching. The data first undergo a process of radio frequency interference (RFI) excision; the first stage of which is to flag channels containing bright, repetitive signals. Secondly, the time-series corresponding to the average of all channels, without any correction for dispersion applied, is searched for bright bursts; any found are removed from the data; in this way non-dispersed terrestrial bursts are rejected. There are channels that always contain RFI at Parkes; these are flagged automatically. Typically around 190 channels are flagged.

The data are then "dedispersed" by correcting for delays corresponding to approximately 1400 DM values ($0 < \mathrm{DM} < 2000$ cm^{-3} pc) before averaging all channels. The resultant one-dimensional time-series are then searched for significant peaks with a series of matched filters of increasing width; these filters improve sensitivity to bursts wider than the sampling resolution. Signals with signal-to-noise ratio (SNR) < 6 are disregarded to reduce the number of spurious candidates due to thermal noise (*20*). In this way candidate single pulses are generated. The HTRU survey is less sensitive to high-DM single pulses because of the dispersive spread within one channel is increased, this cannot be corrected for (*20*).

At this stage the candidates resulting from the 13 simultaneous beams of the receiver undergo a multibeam rejection routine. This involves removing candidate pulses appearing in more than 9 beams; this is done in an effort to reject RFI, and in particular perytons, which appear in all beams (*8*). A final cut (DM > 100 cm^{-3} pc and SNR > 9) is applied before human inspection of all remaining candidates.

Pulse Fitting Method

The full bandwidth was divided into a number of sub-bands. Each sub-band was convolved with a template with a scattering tail using a characteristic scattering time. This scattering time was determined from a value at a reference frequency, 1 GHz, which was scaled according to $\tau \propto \nu^{\beta}$ to each sub-band center frequency. Note τ is the broadening due to scattering, and is different from the measured width, *W*, which may include intrinsic and other broadening effects. Using the arrival time of the burst at reference frequency ν_0, the arrival time at a frequency ν was scaled according to a dispersion law $\delta t \propto \mathrm{DM} \cdot \nu^{\alpha}$. The parameters $\delta t(\nu_0), \tau(\nu_0)$, DM, α, and β, were determined in a least-square fit using the SIMPLEX and MIGRAD algorithms from CERN's MINUIT package (*30*). Uncertainties were derived using the MINUIT algorithm to explore the error matrix, which also attempts to account for correlations between parameters.

An overall baseline and amplitude of the scattered pulse of each sub-band were also treated as free parameters to be fit. Before the final step, these parameters were kept fixed to the previous best-fit value.

Supplementary Text

Fitting Results

FRB 110220 has the largest SNR and allows the determination of all parameters as described above. Here, the band was divided into 16 sub-bands, two sub-bands at the top and one at the bottom of the frequency range were excluded from the fit, as, due to an instrumental roll-over of the bandpass, SNR was low. The resulting 13 sub-bands, with 25 MHz each, are frequency-averaged versions of the original 0.39 MHz-wide channels in each sub-band. The time resolution was rebinned to 0.512 ms per sample. The fitting results are consistent with an unresolved pulse at infinite frequency, so a Gaussian pulse was used as a template. The width of the pulse was varied according to the dispersion smearing at each sub-band, ranging from 0.87 ms (1.7 samples) to 1.80 ms (3.5 samples). To take this variation of the width into account before convolving with the scattering tail, the fitting was performed for various widths in this range. In the case of α these fits indicated a small spread of values about that given in Table 1, the uncertainty specified is the spread of these values; the statistical uncertainty on each fit was significantly smaller, as indicated in Figure S1. For β the spread of values was of similar magnitude to the statistical uncertainty on a single fit; in this case the uncertainty of the value in Table 1 reflect the spread of β and the statistical uncertainty on a single fit which are of a similar magnitude.

Alternatively, the template could have been spread by dispersion within each sub-band, but as the dispersion law was included in the fit, and as the true intrinsic shape of the pulse is not known, we used variation of the template width as a means to explore the dependence of our results on template width.

All of the intrinsic pulse width fits indicated a similar χ^2 including unresolved (limited by the downsampled temporal resolution). The marginally best χ^2 was obtained for a dispersed (within the sub-bands) template width of 2 bins (1.02 ms), i.e $\chi^2 = 26316$ for 26605 degrees of freedom, corresponding to a reduced χ^2 of 0.989,

indicating an excellent fit (see Fig. S1). Taking the dispersion smearing into account, this suggests an intrinsic width of less than 1.02 ms. Overall, the fit is consistent with the expectation from a cold plasma law and interstellar scattering, confirming the astrophysical nature of FRB 110220 (see Fig. S1).

FRBs 110627 and 120127 are too weak for a detailed analysis. FRB 110703 was weaker than FRB 110220 and had to be frequency collapsed to just eight sub-bands of 50 MHz bandwidth, 2 sub-bands were excluded at the top and bottom of the band. The rebinning factor in time was also larger than for FRB 110220 in order to achieve sufficient SNR. We found, for the resulting 3.512 ms resolution, the pulse was consistent with not having been scattered. Attempts to increase the time resolution in order to resolve the pulse resulted in an SNR too low to obtain reliable fit results. We therefore only adapted one template width, namely 0.57 bins (2.01 ms), which corresponds to the DM smearing at the lowest frequency channel, and fitted in the final step only for $\delta t(\nu_0)$, DM, and α. Again, the results support the astrophysical nature of the pulse. Note in Table 1 the uncertainty on α is taken to be the uncertainty for FRB 110220. We do this because we have not fit for β simply because there is insufficient SNR; there is likely some covariance between α and β which is implicit in the value derived for α.

RFI

It is important and difficult to distinguish non-repeating radio sources from RFI to be sure of an astronomical origin. Knowledge of well-studied astronomical signals of similar type, or which have undergone similar propagation effects, inform us about what to expect from such a signal. While FRBs are not from pulsars they share the characteristics of broadband coherent emission that has propagated through turbulent ionized material. The effects of this propagation on pulses emitted by pulsars are well studied, and the common observables are well understood. The FRBs are measured to obey astronomical dispersive delay and scattering to a high accuracy; it seems unlikely that a man-made source, especially emitting in a protected band, would so accurately reproduce this behavior. The broadband nature of the bursts also rules out the majority of the RFI environment, which consists of short-duration non-dispersed narrowband pulses.

The ~25 now-reported perytons (*8, 19, 31*) are characterized by 20–50 ms wide, symmetric, swept-frequency pulses that imperfectly mimic a $\delta t \propto \nu^{-2}$ dispersive sweep. Perytons' equivalent DM distribution has a peak near 375 cm^{-3} pc and a negative skew (the range is ~ 200–420 cm^{-3} pc). Perytons are easily recognized by their appearance in all beams of the multibeam receiver, indicating a sidelobe detection. The similarity of these peryton properties with the sweep rate and duration of the FRB 010724 led to the suggestion it might be a peryton during which the telescope was directly pointed at the source, however its celestial or terrestrial origin cannot yet be conclusively determined (*8*). This is not the case for the four FRBs presented here, which have a much larger (and apparently random) DM range, adhere to a dispersive sweep to high precision, and three of which are a factor of > 3 shorter duration than all known perytons. Furthermore, the fast-rise and exponential-tail profile of FRB 110220 makes a clear case for cold plasma propagation; FRB 010724, while displaying frequency-dependent pulse broadening, did not have clear asymmetry.

Because spatial filters are powerful discriminators of local RFI, the current search system rejects signals that are significantly detected in nine or more of the telescope's 13

beams. Therefore, we are likely filtering out a large number of perytons expected to appear in the HTRU survey. Thus far, two perytons (sufficiently weak to not be detected in all beams due to receiver gain variations) have been discovered in HTRU data from the year 2010. This indicates that perytons are still occurring at the telescope, however it also confirms that perytons still exhibit the same imperfectly-dispersed, symmetric form, with <DM> ~ 375 cm^{-3} pc and <W> ~ 30 ms. Like all previously-detected perytons, the new perytons are not obvious analogs to FRBs.

DM contributions

Signals that originate in the MW, and are dispersed by the interstellar medium (ISM), are not redshifted. In this case, $\mathrm{DM} = \int n_e \cdot dl$ assumes *dl* is constant during signal propagation. The MW delay contributions are therefore constant with source redshift for a given line of sight because the frequencies sampled at the telescope are essentially the same as they were when they reached the edge of the MW. The DM contribution from the MW is highly dependent on Galactic latitude, at high Galactic latitudes there is little material along the line of sight and typical MW DMs are small. FRBs at high Galactic latitudes exhibit extremely high DMs that are clearly anomalous to the Galactic pulsar population: a distinct indication of their extragalactic nature (see Fig. S2).

If the sources are located in a galactic disk, and the MW model of the free electron distribution (*10*) is representative of the host galaxy, then $\mathrm{DM_{Host}}$ is dictated by the viewing angle. Considering a median inclination angle, $i = 60°$, the galaxy's ISM causes $\mathrm{DM_{Host}} \approx 100\ \mathrm{cm^{-3}}$ pc ; therefore, the majority of $\mathrm{DM_E}$ would be due to the IGM.

It may also be possible that an intervening galaxy along the line of sight to the source is an additional source of dispersion. As the measured dispersion is an integrated effect the presence of an intervening galaxy would reduce the contribution to the total DM from the IGM. This intervening galaxy contribution would be subject to the same conditions regarding inclination as described for sources located in a galactic disk. If there were a contribution from an intervening galaxy, this would, of course, equate to a closer source. We note the probability of an intervening source within $z < 1$ is less than 0.05 (*16*).

When considering dispersion caused by the IGM and a host it becomes necessary to take into account the expansion of the universe and the fact that the radiation that makes up the pulse is affected by the stretching of space-time. An important manifestation is that the radiation that underwent dispersion in a host galaxy was at a higher frequency, $\nu \rightarrow \nu(1+z)$. Since the dispersive delays follow $\delta t \propto \nu^{-2}$, the *observed* delay due to a given $\mathrm{DM_{Host}}$ decreases with increasing redshift. The same argument applies to dispersive delays from the IGM where the electron density and length-scale both depend on redshift. The total delay due to the IGM is found by integrating along the line of sight to a source. By combining this with host and MW delay contributions a total delay can be found and a redshift calculated (see Fig. S3).

FRB locations

Detailed attempts to constrain the position of FRB 110220 by using its non-detection in the other beams does not produce a better localization than the HPBW and is not simply described by a single quantity. Positioning is further complicated because the beam shape is frequency dependent – it is wider for lower frequencies. This imparts an apparent spectral index to a source located away from the beam center. Combining this with the unknown intrinsic spectral index there is little constraint on the location within the beam. For these reasons the HPBW is used while recognizing the difficulty in knowing the true position.

There are 15, 56, 30, and 54 cataloged galaxies within the HPBW for FRB 110220, 110627, 110703, and 120127 respectively. Some of these have measured redshifts of $z = 0.02, 0.6$. If located in one of these galaxies then DM_{IGM} would be either 17 cm^{-3} pc ($z = 0.02$) or 570 cm^{-3} pc ($z = 0.6$), as such a significant fraction of DM_E would be due to the host. In these directions there are almost certainly as yet undiscovered galaxies at other redshifts.

The empirical relationship between DM and scattering (*15*) may be used to constrain the redshift to $z > 0.11$

In addition to looking at galaxies in the field of view we also looked for temporally associated GRBs or x-ray transients. Gamma-ray and X-ray telescopes have all-sky monitors however we did not find any cataloged event (NASA HEASARC) which could be related to any of the FRBs in this paper. The Astronomers Telegram was also checked for possibly associated events; none were found.

Energetics

The energy released, E, (see Table 1) is calculated as the total energy of the burst at the source. The energy released, $E \sim F \cdot D^2 \cdot BW$, where F is the fluence, D is the cosmological luminosity distance, and BW is the bandwidth at the source. Note that emission is not assumed isotropic, instead a beam of 1 steradian is used for simplicity. In the case of these FRBs, where there is significant redshift, the width, distance, and bandwidth must be corrected to account for cosmological redshift. These corrections have been made for the E values in Table 1. As the measurement of spectral index is inconclusive we have assumed it to be flat (Fig. S4) and do not extrapolate beyond the observing band.

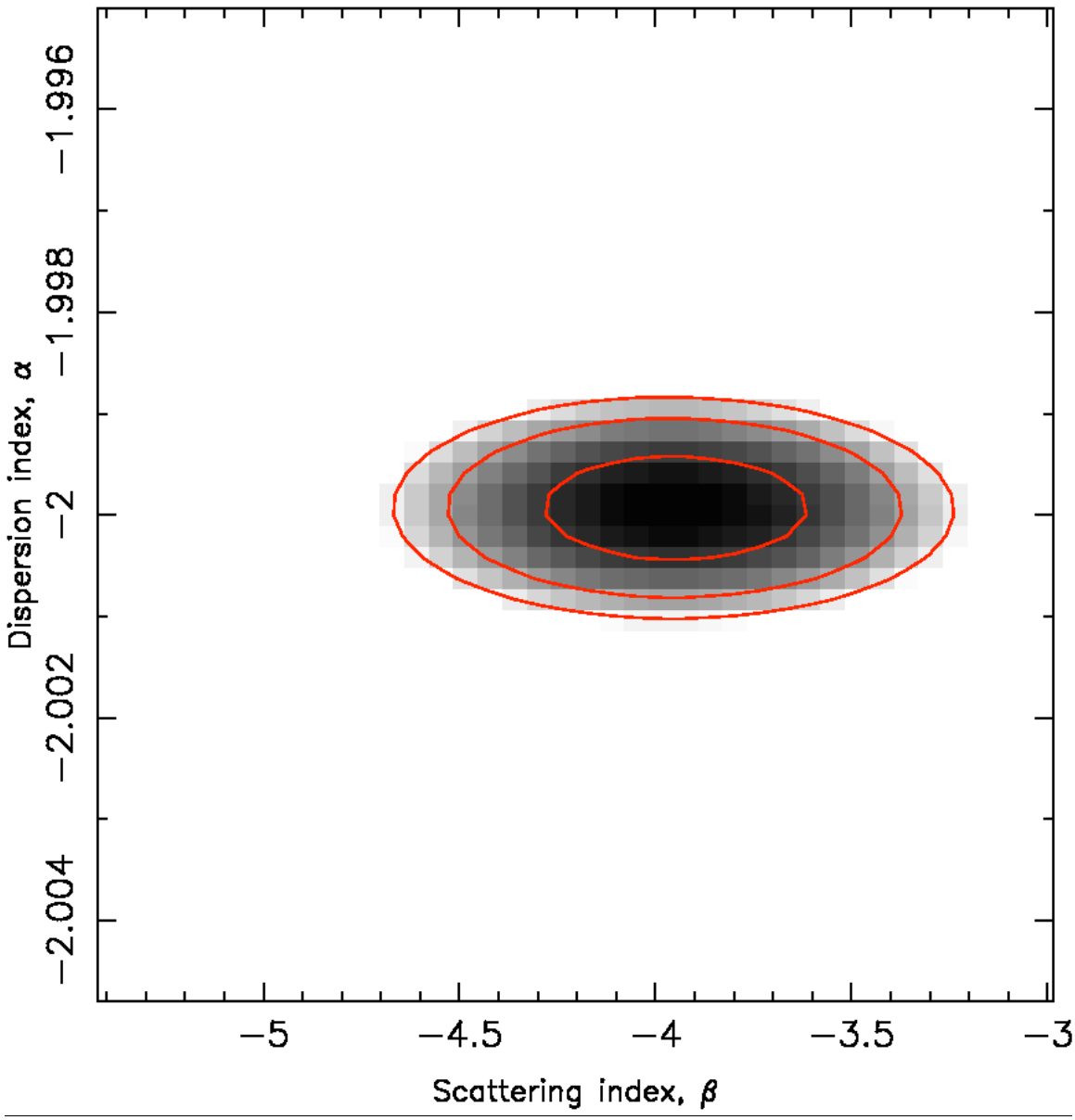

Fig. S1.

A grayscale plot showing the reduced-χ^2 as a function of dispersion index, α, and scattering index, β. The concentric lines indicate the 1-, 2-, and 3-σ confidence intervals about the best values (see Table 1). Note this figure corresponds to the fit with a smeared intrinsic width of 2 bins, 1.02 ms, not the ranges indicated in Table 1.

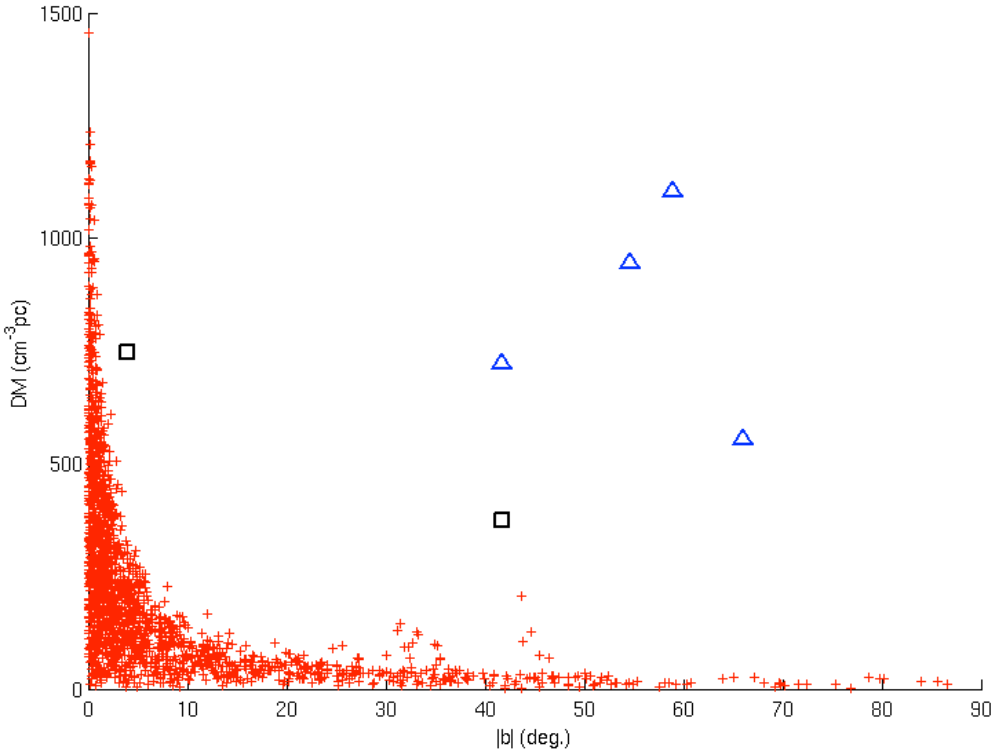

Fig. S2.

Measured DM for FRBs and known pulsars is plotted against the magnitude of Galactic latitude. The FRBs from this paper are shown as blue triangles, FRB 010621 and 010724 are shown as black squares, pulsars are indicated by red '+' symbols. The FRBs exhibit significantly higher dispersion than pulsars at similar separations from the Galactic plane. The pulsars with an apparent dispersion excess located at $30° < |b| < 45°$ are in the Magellanic clouds which provide an additional source of free electrons and dispersion.

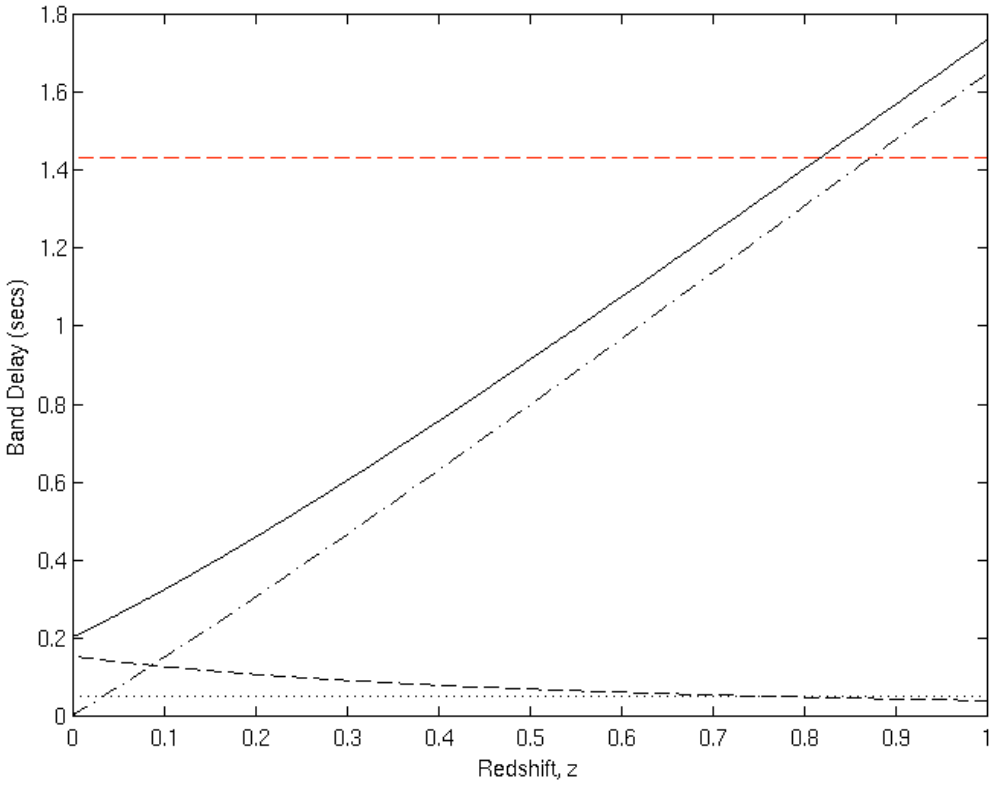

Fig. S3

Modelled dispersive delay (in seconds) across the observing band of the HTRU survey is shown plotted against redshift. The flat dashed line indicates the delay across the observing band for FRB 110220. The dotted line is the MW contribution and is constant irrespective of the redshift of the source, the dot-dashed line is the delay due to the IGM, the curved dashed line is the delay contribution from a host galaxy with $DM_{Host} = 100$ cm^{-3} pc, and the solid line is the sum of the IGM, host and MW contributions. When the sum of contributions is equal to the measured delay the redshift is inferred.

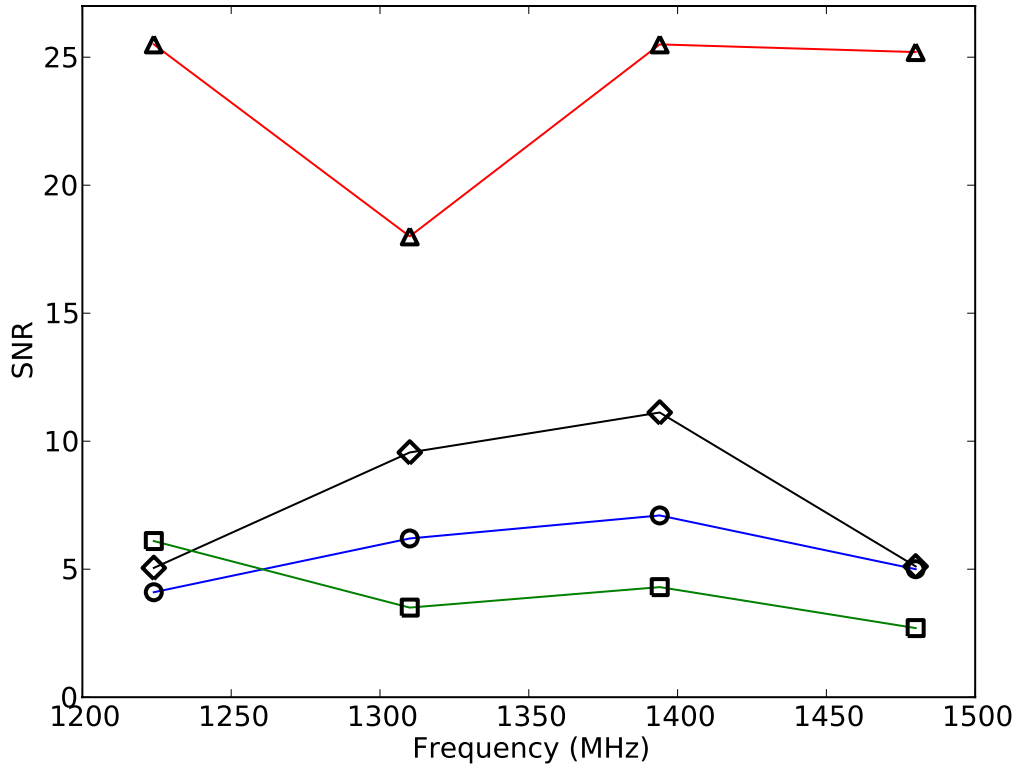

Fig. S4

The SNRs of the FRBs (110220: triangles, 110627: circles, 110703: diamonds, 120127: squares). For each the total band has been split into four 100-MHz sub-bands and the SNR of the pulse in each measured.

Table S1.

The parameters detailing the HTRU high-latitude southern survey, which covers the sky visible to the Parkes radio telescope. The areas quoted correspond to the total area observed and processed at the time of writing; the area of a single beam, 0.08 deg^2, is calculated using the half-power beam-width at 1.3 GHz.

Region	High-Latitude
Coverage	Declination < +10°
Pointing Length (s)	270
Sampling time (μs)	64
Band Center Frequency (MHz)	1382
Channel Bandwidth (MHz)	0.390625
Number of channels	1024
Beams at completion	443287
Beams Processed	95670
FRBs Found	4
Completed Area ($deg.^2$)	4078
Completed Time (days)	298
Completed Area (skys, 4π sr)	0.098
Completed Time (years)	0.82

References and Notes

1. M. J. Keith, A. Jameson, W. Van Straten, M. Bailes, S. Johnston, M. Kramer, A. Possenti, S. D. Bates, N. D. R. Bhat, M. Burgay, S. Burke-Spolaor, N. D'Amico, L. Levin, P. L. McMahon, S. Milia, B. W. Stappers, The High Time Resolution Universe Pulsar Survey - I. System configuration and initial discoveries. *Mon. Not. R. Astron. Soc.* **409**, 619–627 (2010). doi:10.1111/j.1365-2966.2010.17325.x

2. Materials and methods are available as supplementary material on *Science* Online.

3. J. M. Cordes, *SKA Memo Ser.* **97**, 1 (2009).

4. D. R. Lorimer, M. Bailes, M. A. McLaughlin, D. J. Narkevic, F. Crawford III, A bright millisecond radio burst of extragalactic origin. *Science* **318**, 777–780 (2007); 10.1126/science.1147532. doi:10.1126/science.1147532 Medline

5. E. F. Keane, B. W. Stappers, M. Kramer, A. G. Lyne, On the origin of a highly dispersed coherent radio burst. *Mon. Not. R. Astron. Soc.* **425**, L71–L75 (2012). doi:10.1111/j.1745-3933.2012.01306.x

6. K. W. Bannister, T. Murphy, B. M. Gaensler, J. E. Reynolds, Limits on prompt, dispersed radio pulses from gamma-ray bursts. *Astrophys. J.* **757**, 38 (2012). doi:10.1088/0004-637X/757/1/38

7. E. Rubio-Herrera, B. W. Stappers, J. W. T. Hessels, R. Braun, A search for radio pulsars and fast transients in M31 using the Westerbork Synthesis Radio Telescope. *Mon. Not. R. Astron. Soc.* **428**, 2857–2873 (2013). doi:10.1093/mnras/sts205

8. S. Burke-Spolaor, M. Bailes, R. Ekers, J.-P. Macquart, F. Crawford III, Radio bursts with extragalactic spectral characteristics show terrestrial origins. *Astrophys. J.* **727**, 18 (2011). doi:10.1088/0004-637X/727/1/18

9. The Lorimer burst is designated as FRB 010724; this date is a correction to that in the original paper.

10. J. M. Cordes, T. J. W. Lazio (2002), http://arxiv.org/abs/astroph/0207156.

11. J. S. Deneva, J. M. Cordes, T. J. W. Lazio, Discovery of three pulsars from a galactic center pulsar population. *Astrophys. J.* **702**, L177–L181 (2009). doi:10.1088/0004-637X/702/2/L177

12. K. Ioka, The cosmic dispersion measure from gamma-ray burst afterglows: Probing the reionization history and the burst environment. *Astrophys. J.* **598**, L79–L82 (2003). doi:10.1086/380598

13. S. Inoue, Probing the cosmic reionization history and local environment of gamma-ray bursts through radio dispersion. *Mon. Not. R. Astron. Soc.* **348**, 999–1008 (2004). doi:10.1111/j.1365-2966.2004.07359.x

14. I. P. Williamson, *Mon. Not. R. Astron. Soc.* **157**, 55 (1972).

15. N. D. R. Bhat, J. M. Cordes, F. Camilo, D. Nice, D. R. Lorimer, Multifrequency observations of radio pulse broadening and constraints on interstellar electron density microstructure. *Astrophys. J.* **605**, 759–783 (2004). doi:10.1086/382680

16. R. C. Roeder, R. T. Verreault, The screening of distant objects in universes with positive cosmological constant. *Astrophys. J.* **155**, 1047 (1969). doi:10.1086/149933

17. H. Isliker, A. O. Benz, *Astron. Astrophys. Suppl. Ser.* **104**, 145 (1994).

18. R. N. Manchester, A. G. Lyne, F. Camilo, J. F. Bell, V. M. Kaspi, N. D'Amico, N. P. F. McKay, F. Crawford, I. H. Stairs, A. Possenti, M. Kramer, D. C. Sheppard, The Parkes Multi-Beam Pulsar Survey - I. Observing and data analysis systems, discovery and timing of 100 pulsars. *Mon. Not. R. Astron. Soc.* **328**, 17–35 (2001). doi:10.1046/j.1365-8711.2001.04751.x

19. M. Bagchi, A. C. Nieves, M. McLaughlin, A search for dispersed radio bursts in archival Parkes Multibeam Pulsar Survey data. *Mon. Not. R. Astron. Soc.* **425**, 2501–2506 (2012). doi:10.1111/j.1365-2966.2012.21708.x

20. S. Burke-Spolaor, M. Bailes, S. Johnston, S. D. Bates, N. D. R. Bhat, M. Burgay, N. D'Amico, A. Jameson, M. J. Keith, M. Kramer, L. Levin, S. Milia, A. Possenti, B. Stappers, W. van Straten, The High Time Resolution Universe Pulsar Survey - III. Single-pulse searches and preliminary analysis. *Mon. Not. R. Astron. Soc.* **416**, 2465–2476 (2011). doi:10.1111/j.1365-2966.2011.18521.x

21. D. A. Frail, S. R. Kulkarni, R. Sari, S. G. Djorgovski, J. S. Bloom, T. J. Galama, D. E. Reichart, E. Berger, F. A. Harrison, P. A. Price, S. A. Yost, A. Diercks, R. W. Goodrich, F. Chaffee, Beaming in gamma-ray bursts: Evidence for a standard energy reservoir. *Astrophys. J.* **562**, L55–L58 (2001). doi:10.1086/338119

22. D. S. Madgwick, O. Lahav, I. K. Baldry, C. M. Baugh, J. Bland-Hawthorn, T. Bridges, R. Cannon, S. Cole, M. Colless, C. Collins, W. Couch, G. Dalton, R. De Propris, S. P. Driver, G. Efstathiou, R. S. Ellis, C. S. Frenk, K. Glazebrook, C. Jackson, I. Lewis, S. Lumsden, S. Maddox, P. Norberg, J. A. Peacock, B. A. Peterson, W. Sutherland, K. Taylor, The 2dF Galaxy Redshift Survey: Galaxy luminosity functions per spectral type. *Mon. Not. R. Astron. Soc.* **333**, 133–144 (2002). doi:10.1046/j.1365-8711.2002.05393.x

23. E. O. Ofek, Soft gamma-ray repeaters in nearby galaxies: Rate, luminosity function, and fraction among short gamma-ray bursts. *Astrophys. J.* **659**, 339–346 (2007). doi:10.1086/511147

24. K. Hurley, S. E. Boggs, D. M. Smith, R. C. Duncan, R. Lin, A. Zoglauer, S. Krucker, G. Hurford, H. Hudson, C. Wigger, W. Hajdas, C. Thompson, I. Mitrofanov, A. Sanin, W. Boynton, C. Fellows, A. von Kienlin, G. Lichti, A. Rau, T. Cline, An exceptionally bright flare from SGR 1806-20 and the origins of short-duration gamma-ray bursts. *Nature* **434**, 1098–1103 (2005). doi:10.1038/nature03519 Medline

25. B. M. S. Hansen, M. Lyutikov, Radio and X-ray signatures of merging neutron stars. *Mon. Not. R. Astron. Soc.* **322**, 695–701 (2001). doi:10.1046/j.1365-8711.2001.04103.x

26. M. J. Rees, A better way of searching for black-hole explosions? *Nature* **266**, 333–334 (1977). doi:10.1038/266333a0

27. R. Diehl, H. Halloin, K. Kretschmer, G. G. Lichti, V. Schönfelder, A. W. Strong, A. von Kienlin, W. Wang, P. Jean, J. Knödlseder, J. P. Roques, G. Weidenspointner, S. Schanne, D. H. Hartmann, C. Winkler, C. Wunderer, Radioactive 26Al from massive stars in the Galaxy. *Nature* **439**, 45–47 (2006). doi:10.1038/nature04364 Medline

28. A. E. Egorov, K. A. Postnov, On the possible observational manifestation of the impact of a supernova shock on the neutron star magnetosphere. *Astron. Lett.* **35**, 241–246 (2009). doi:10.1134/S1063773709040033

29. N. Spergel, L. Verde, H. V. Peiris, E. Komatsu, M. R. Nolta, C. L. Bennett, M. Halpern, G. Hinshaw, N. Jarosik, A. Kogut, M. Limon, S. S. Meyer, L. Page, G. S. Tucker, J. L. Weiland, E. Wollack, E. L. Wright, First-year *Wilkinson Microwave Anisotropy Probe* (*WMAP*) observations: Determination of cosmological parameters. *Astrophys. J. Suppl. Ser.* **148**, 175–194 (2003). doi:10.1086/377226

30. MINUIT physics analysis tool for function minimization, available at http://seal.web.cern.ch/seal/work-packages/mathlibs/minuit/home.html.

31. J. Kocz, M. Bailes, D. Barnes, S. Burke-Spolaor, L. Levin, Enhanced pulsar and single pulse detection via automated radio frequency interference detection in multipixel feeds. *Mon. Not. R. Astron. Soc.* **420**, 271–278 (2012). doi:10.1111/j.1365-2966.2011.20029.x